nature physics

LETTERS

https://doi.org/10.1038/s41567-018-0241-6

A passive photon–atom qubit swap operation

Orel Bechler[1,3], Adrien Borne[1,3], Serge Rosenblum[1,3], Gabriel Guendelman[1], Ori Ezrah Mor[1], Moran Netser[1], Tal Ohana[1], Ziv Aqua[1], Niv Drucker[1], Ran Finkelstein[1], Yulia Lovsky[1], Rachel Bruch[1], Doron Gurovich[1], Ehud Shafir[1,2] and Barak Dayan[1*]

Deterministic quantum interactions between single photons and single quantum emitters are a vital building block towards the distribution of quantum information between remote systems[1–4]. Deterministic photon–atom state transfer has previously been demonstrated with protocols that include active feedback or synchronized control pulses[5–10]. Here we demonstrate a passive swap operation between the states of a single photon and a single atom. The underlying mechanism is single-photon Raman interaction[11–15]—an interference-based scheme that leads to deterministic interaction between two photonic modes and the two ground states of a Λ-system. Using a nanofibre-coupled microsphere resonator coupled to single Rb atoms, we swap a photonic qubit into the atom and back, demonstrating fidelities exceeding the classical threshold of 2/3 in both directions. In this simultaneous write and read process, the returning photon, which carries the readout of the atomic qubit, also heralds the successful arrival of the write photon. Requiring no control fields, this single-step gate takes place automatically at the timescale of the atom's cavity-enhanced spontaneous emission. Applicable to any waveguide-coupled Λ-system, this mechanism, which can also be harnessed to construct universal gates[16,17], provides a versatile building block for the modular scaling up of quantum information systems.

While teleportation protocols[18–20] provide one possible route for linking separate quantum modules, considerable effort is currently invested towards the realization of a direct state transfer between photonic and material qubits, especially within the field of cavity quantum electrodynamics[21,22]. Already at moderate fidelities and efficiencies[23], such photonic links enable scalable architectures for distributed quantum information processing based on interconnected compact modules[1–4]. Deterministic two-way transfer between photonic and material qubits had so far been demonstrated with active protocols that include auxiliary control fields—from stimulated Raman adiabatic passage[6,7], to the Duan and Kimble protocol[5]. Specifically, in the Duan and Kimble protocol, the 'native gate'—the naturally occurring interaction between the photon and the atom—is a controlled-phase gate between the photon and the atom. Classical laser pulses are then used to measure and manipulate the state of the atom, thereby attaining a variety of other interactions, such as photon–atom state transfer[7,10] and photon–photon gates[8,9,24].

Here we demonstrate an alternative, passive scheme whose native interaction is the swap gate—a direct, one-step mutual exchange of quantum states between photonic and material qubits. The underlying mechanism, single-photon Raman interaction (SPRINT), harnesses quantum interference to 'force' a single Λ-type quantum emitter to end up in one of its two ground states depending on the input mode of a single photon. Initially considered in ref. [25] and analysed in a series of theoretical works[15,26–28], this mechanism was first realized experimentally to create an all-optical single-photon switch[11], and to demonstrate deterministic extraction of a single photon from optical pulses[13]. The effect was also demonstrated in superconducting circuits, where it enabled frequency conversion of microwave fields[12] and highly efficient detection of single microwave photons[14].

The configuration that leads to SPRINT includes a Λ-system in which each of its two transitions is coupled, with the same cooperativity C, to a different mode of an optical waveguide. As depicted in Fig. 1a, assuming the Λ-system is initiated at the $|\downarrow_z\rangle_a$ ground state, and that loss and coupling to free-space modes (at rate γ) are much smaller than the coupling rate Γ to the waveguide modes (that is, $C=\Gamma/\gamma\gg 1$), the radiation from the system interferes destructively with any incoming light in mode $\hat{a}$, eliminating the outgoing field in this mode. An incoming photon is therefore diverted to mode $\hat{b}$, leading to a Raman transition of the atom to the state $|\uparrow_z\rangle_a$, which is a dark state for mode $\hat{a}$. Accordingly, once in this state, the system lets photons in mode $\hat{a}$ continue undisturbed (Fig. 1b). Evidently, the photon and the Λ-system play symmetric roles: the incoming mode of the photon dictates the final state of the Λ-system, and the initial state of the Λ-system dictates the output mode of the photon. As SPRINT is coherent, this description holds for superposition states as well. This means that it essentially performs as a quantum swap gate between the photonic qubit (encoded in a superposition of the two input modes) and the material qubit (encoded in its two ground states). The swap operation is unitary, in which the (arbitrary) initial state of the atom is not lost by interaction with classical fields, but transferred to the outgoing photon simultaneously with the 'writing' of the new state carried by the incoming photon.

Our experimental implementation consists of single ^{87}Rb atoms coupled to an ultrahigh-quality microsphere resonator, which is temperature-tuned to be resonant with the $F=1\rightarrow F'=1$ transition of the ^{87}Rb D_2 line. The atoms are repeatedly (1 Hz) trapped in a magneto-optical trap, and then cooled to ~7 μK and dropped onto the microsphere placed ~7 mm below. The rare event of an atom falling through the evanescent field of one of the resonator's transverse-magnetic whispering-gallery modes (WGMs) is detected by a fast series of pulses before and after the experiment is carried out, ensuring that the atom resides within the optical mode throughout the experimental sequence (see Methods). Light is evanescently coupled into and out of the resonator using a tapered nanofibre (Fig. 1c). The optical set-up has two possible configurations—with and without a 50:50 beamsplitter. Without the beamsplitter, the two input/output ports couple light to opposite directions of the tapered

[1]AMOS and Department of Chemical Physics, Weizmann Institute of Science, Rehovot, Israel. [2]Present address: Soreq NRC, Yavne, Israel. [3]These authors contributed equally to this work: Orel Bechler, Adrien Borne, Serge Rosenblum. *e-mail: barak.dayan@weizmann.ac.il

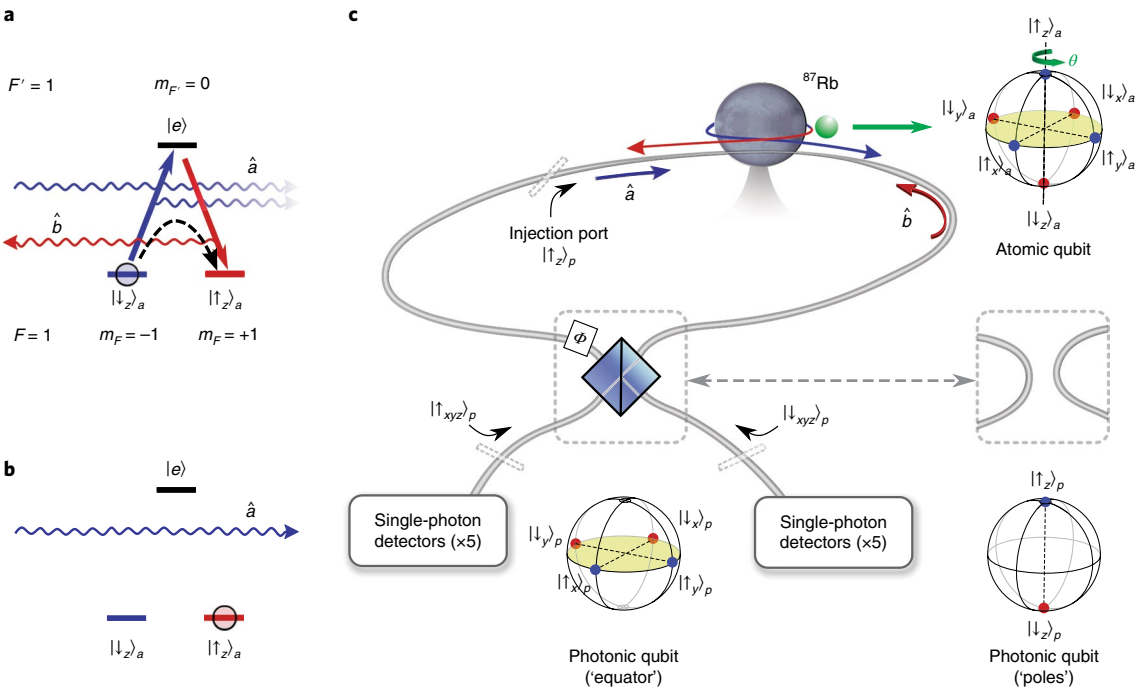

Fig. 1 | The SPRINT scheme and experimental apparatus. a, A material Λ-system in which each transition is coupled to a different single optical mode ($\hat{a}$,$\hat{b}$). Incoming light from mode $\hat{a}$ interacts with the system, initially in ground state $|\downarrow_z\rangle_a$ (blue). Destructive interference (blue gradient fade) in this mode forces the system to radiate only to mode $\hat{b}$, thereby toggling the system to ground state $|\uparrow_z\rangle_a$ (red). **b**, In its toggled, dark state, the system is transparent to light in mode $\hat{a}$. As evident, the input photonic mode determines the resulting state of the material system and vice versa. **c**, Our experimental realization includes a single ^{87}Rb atom (green sphere) that interacts with a transverse-magnetic mode of a microsphere resonator. The input/output interface is provided by an optical nanofibre in which mode $\hat{a}$ (blue) propagates from left to right, and mode $\hat{b}$ (red) from right to left. Guiding light into and out of the input and output ports of the nanofibre is achieved by 97:3 beamsplitters, used to attenuate the input weak coherent pulses and highly transmit the output photons. Four input ports are available: $|\uparrow_z\rangle_p$,$|\downarrow_z\rangle_p$ (corresponding to the 'pole' states of the photonic qubit Bloch sphere) and their superposition ('equator') states, accessible using the two inputs of a 50:50 beamsplitter combined with a Pockels cell to control their relative phase (Φ). The random location of the atom along the circumference of the resonator leads to relative rotation of the atomic Bloch sphere compared to the photonic Bloch sphere (θ, green arrow) that varies between different experimental runs. The 'injection' port on the left side enables probing the atom by sending a photon with a fixed photonic state $|\uparrow_z\rangle_p$. Outputs are split using fibre couplers to ten single-photon counting modules (SPCMs), five on each output port.

fibre, corresponding to the 'poles' of the photonic qubit Bloch sphere, $|\uparrow_z\rangle_p$ and $|\downarrow_z\rangle_p$. With the beamsplitter, along with an electro-optic phase modulator (Pockels cell), the two input/output ports correspond to the 'equator' states on the photonic Bloch sphere—the superpositions $(|\downarrow_z\rangle_p + e^{i\Phi}|\uparrow_z\rangle_p)/\sqrt{2}$ and $(|\downarrow_z\rangle_p - e^{i\Phi}|\uparrow_z\rangle_p)/\sqrt{2}$, with the phase ϕ set by the Pockels cell.

The counter-propagating transverse-magnetic WGMs of the microsphere exhibit nearly opposite circular polarizations[29–31]. This means that the photonic mode $\hat{a}$ drives mostly the atomic $m_F = -1 \rightarrow m_{F'} = 0$ transition, and the mode $\hat{b} = |\downarrow_z\rangle_p$ drives mostly the $m_F = +1 \rightarrow m_{F'} = 0$ transition, with little crosstalk (~4.5%). This system therefore approximates well the desired SPRINT configuration, creating a one-to-one correspondence between the photonic Bloch sphere (being, in fact, the Poincaré sphere, with $|\uparrow_z\rangle_p$, $|\downarrow_z\rangle_p$ corresponding to circular polarizations, and equator states corresponding to linear polarizations) and the atomic Bloch sphere (the states $|\uparrow_z\rangle_a = |F=1, m_F=+1\rangle$, $|\downarrow_z\rangle_a = |F=1, m_F=-1\rangle$ and their superpositions).

Given the intrinsic cavity loss rate $\kappa_i/2\pi = 6$ MHz of the WGM, we follow the analysis of ref. [15] and tune the fibre–cavity coupling rate to be $\kappa_{ex}/2\pi = \sqrt{2\kappa_i/\gamma}\, g = 60$ MHz to maximize the SPRINT performance. This sets the linear loss of the bare cavity to ~30% on resonance. With a coherent atom–cavity coupling rate of $g/2\pi = 27$ MHz and atomic free-space amplitude decay rate of $\gamma/2\pi = 3$ MHz, our system is in the fast-cavity regime for which $\kappa_{ex} > g \gg \kappa_i, \gamma$. The resulting cavity-enhanced spontaneous emission rate in both fibre directions is $\Gamma/2\pi \sim 2g^2/(\kappa_{ex}+\kappa_i) \sim 22$ MHz. With these parameters, the efficiency of the system (namely the photon survival probability) remains ~70% also when coupled to the atom[15].

Demonstrating the feasibility of using SPRINT for photonic quantum communication links requires assessing its performance in mapping an atomic qubit onto an outgoing photon and vice versa. To demonstrate the first part of this twofold task, we first classically prepare the atom in one of the six cardinal points on the Bloch sphere (namely $|\uparrow_{xyz}\rangle_a$ and $|\downarrow_{xyz}\rangle_a$). This is performed by sending a preparation photon and conditioning on a detection event that corresponds to the desired atomic state (see Methods). Next, a weak probe pulse (~0.05 photons on average) is sent to the atom. If a photon is present in the pulse, it should swap its state with that of the atom. Accordingly, the outgoing photon will ideally propagate in a direction dictated only by the initial atomic state, irrespective of the direction of the incoming probe photon. Similarly, the final atomic state should carry no information about the initial one (as required by the no-cloning theorem), but instead should be reset by the incoming photonic state. To determine the fidelity of the output state with the initial atomic state, we analyse it in the basis along which the atomic qubit was prepared.

The results, analysed from ten different experiments involving different pulse combinations (see Methods), are presented in Fig. 2 for two variations of the atom-to-photon swap process. In the first realization, we send the probe photon in the $|\uparrow\rangle$ direction along the same axis in which the atom was initially prepared. The results demonstrate the coherence of the SPRINT mechanism, as it

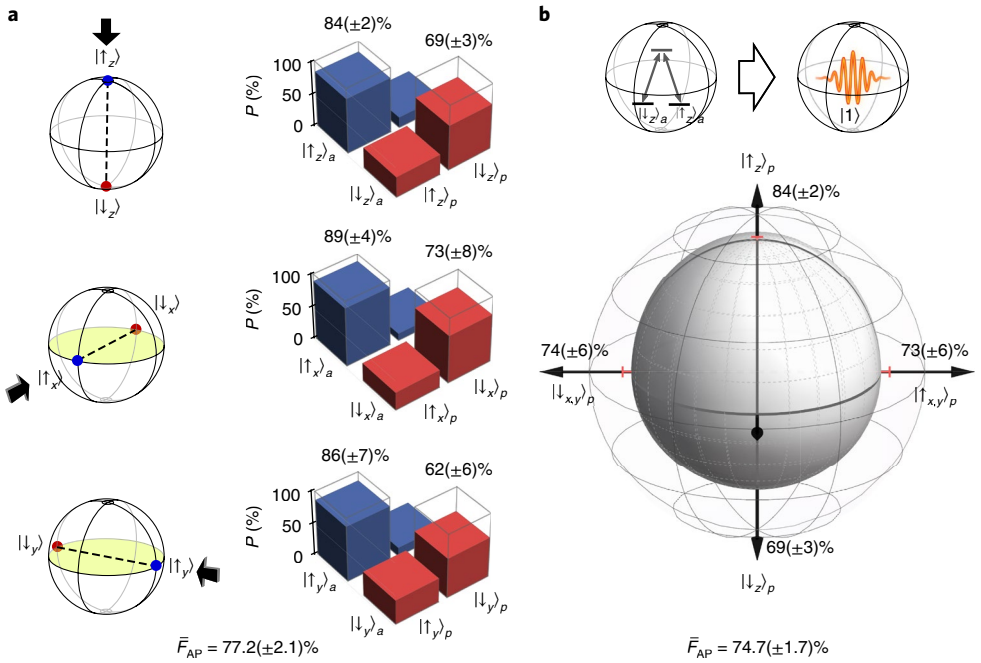

Fig. 2 | Experimental results for the atom-to-photon swap process in two configurations. a, The measured performance of SPRINT for all three axes of the Bloch sphere. In each axis, the atomic state was prepared by sending either $|\uparrow\rangle_p$ or $|\downarrow\rangle_p$. A probe pulse was then sent from the $|\uparrow\rangle_p$ direction of the same axis (black arrows). The bar graphs represent the obtained probability for $|\uparrow\rangle_p$ or $|\downarrow\rangle_p$ (corresponding to transmission or reflection, respectively) at the output for each prepared atomic state (blue or red bars); the empty black boxes signify unit fidelity. The presented results correspond to an average fidelity of $\overline{\mathcal{F}}_{AP}$ = 77.2(±2.1)%. **b**, Measured fidelity of the resulting photonic state for each of the six prepared cardinal states, here with the probe photon always sent from port $|\uparrow_z\rangle_p$. Since the position of the atom varies between experimental runs, equatorial results are presented here on a single axis, representing the average of the *x* and *y* photonic axes. The fidelity averaged over the entire Bloch sphere is $\overline{\mathcal{F}}_{AP}$ = 74.7(±1.7)%.

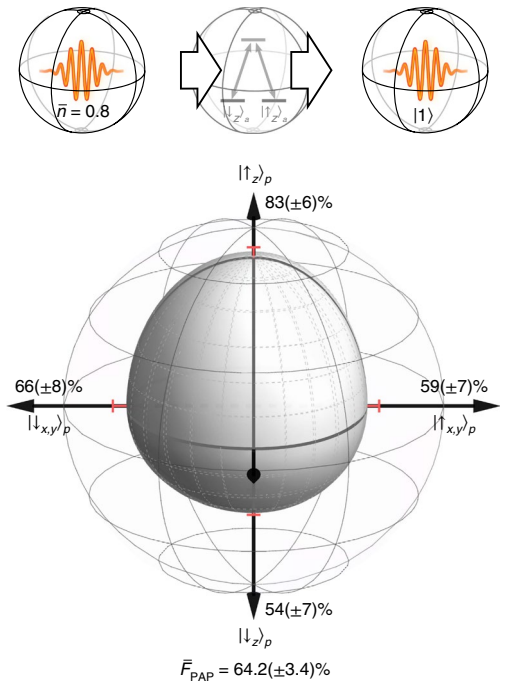

Fig. 3 | Measurement of the photon–atom–photon double-swap fidelity. Measured fidelity of the resulting photonic state for each of the six input photonic cardinal states for the photon–atom–photon double-swap process. A coherent pulse with an average of 0.8 photons 'writes' a photonic qubit on an atom using SPRINT. The state is then extracted as a single photon (by sending a probe pulse from port $|\uparrow_z\rangle_p$) and analysed in the write basis. Similarly to Fig. 2b, results on the equator are averaged on a single *x*, *y* axis. The average fidelity measured for the entire double-swap process is 64.2(±3.4)%.

works similarly for the cardinal states in all of the bases: the probe photon is mostly transmitted (that is, stays in the same mode) if it matches the prepared state of the atomic qubit (T ~ 86%, R ~ 14%), and mostly reflected (that is, switches to the other mode) if it is in the orthogonal state (T ~ 32%, R ~ 68%, see Fig. 2a). For equatorial states, for which the photons reside in a superposition of both fibre directions, transmission is defined as exiting the 50:50 beamsplitter through the same port it came from, whereas a reflected photon exits through the opposite port. The asymmetry in the transmission and reflection fidelities stems from the fact that while for reflection the atom has to actively undergo two subsequent transitions, transmission is passive, resulting from the atom being in a nearly non-interacting dark state. The correspondence between the photonic Bloch sphere (defined by the optical set-up) and the atomic Bloch sphere is set by the atom–cavity coupling g, which has a phase that depends on the location of the atom along the circumference of the resonator. This location, and accordingly the azimuthal phase between the photonic and atomic Bloch spheres, vary from atom to atom (as presented by the green arrow in Fig. 1c). Nonetheless, within each single experimental run (~400 ns), this phase is fixed, leading to a well-preserved coherence of the swapped qubit. In this sense, our experimental results along the equator represent the fidelity of the swap operation for the $|\downarrow\rangle_p$, $|\uparrow\rangle_p$ photonic states (corresponding to the two ports of the beamsplitter, see Fig. 1c), averaged over the varying coupling angles to the atomic qubit. We therefore expect a similar swap fidelity for photonic qubits prepared along the *x* and *y* axes, which is indeed the case. The overall measured atom-to-photon swap fidelity, averaged over all three photonic qubit axes is $\overline{\mathcal{F}}_{AP}$ = 77.2(±2.1)%.

The fact that the axis of the probe photon matches that of the prepared atomic state can potentially bias the atom-to-photon swap process, even though ideally it should affect only the resulting atomic state. To prevent such a bias, we also measured the fidelity of

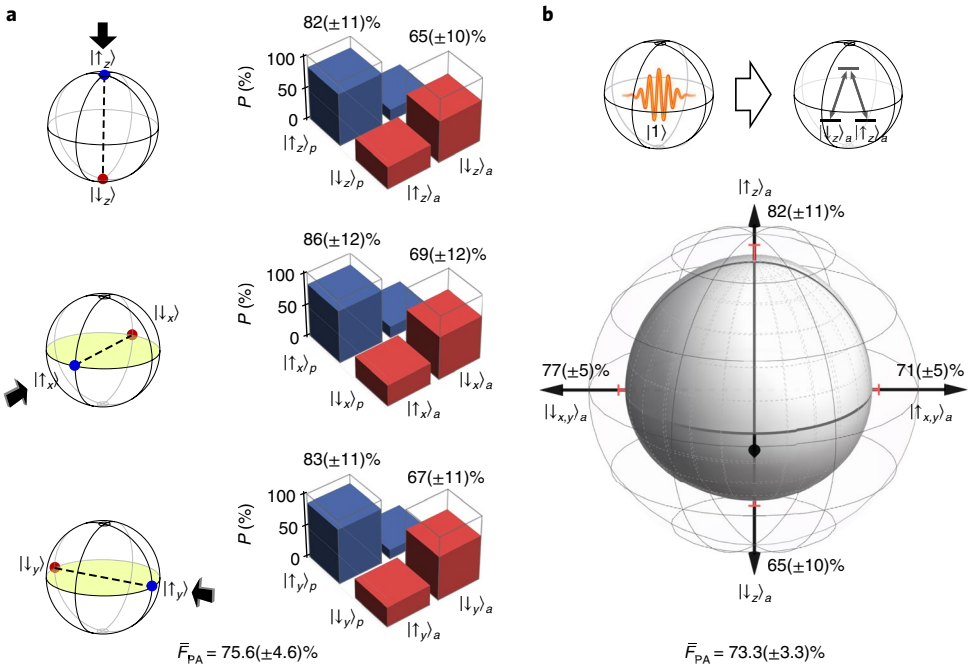

Fig. 4 | Inferred photon-to-atom swap fidelity, presented for a perfect single-photon input qubit. a, Inferred results of the SPRINT process for input photonic states $|\uparrow\rangle_p$ or $|\downarrow\rangle_p$ (blue or red bars) and resulting atomic states on all of the three axes of the Bloch sphere. The empty black boxes signify unit fidelity. The atom is assumed to be prepared at the $|\uparrow\rangle_a$ state on the same axis (black arrows). The presented results correspond to an average fidelity of $\overline{\mathcal{F}}_{PA} = 75.6(\pm4.6)\%$. **b**, Inferred fidelity of the resulting atomic state for each of the six input photonic cardinal states for the photon-to-atom swap process, this time assuming that the atom was always prepared at $|\uparrow_z\rangle_a$. Equator states are averaged onto a single *x*, *y* axis as in Figs. 2 and 3. The resulting fidelity averaged over the entire Bloch sphere is 73.3(±3.3)%.

the atom-to-photon swap process by sending the probe pulse from a fixed direction ($|\uparrow_z\rangle_p$ through the 'injection' port in Fig. 1c), regardless of the preparation basis of the atomic state. The results of these measurements are presented in Fig. 2b, with the equatorial fidelities averaged onto a single axis denoted as *x*, *y*, as any possible differences between *x* and *y* preparations would be averaged out by the shot-to-shot phase discussed above. Note that Fig. 2b strictly presents the measured average overlap between the photonic state that prepared the atom and the one that was swapped out of it. This figure of merit coincides with the process fidelity provided one assumes that these are indeed the principle axes of the process. Also note that since the probe photon is sent in the *z*-axis direction, we do not expect the fidelities on the equator to exhibit the same asymmetry as on the poles, as they result from a combination of both reflective and transmissive SPRINT processes. The measured atom-to-photon fidelity averaged over the entire sphere is $\overline{\mathcal{F}}_{AP} = 74.7(\pm1.7)\%$.

To evaluate the fidelity of the swap operation in the other direction (that is, the photon-to-atom state transfer), we conducted a double, swap-in–swap-out experiment by sending 'write' pulses (~0.8 photons on average) with the six possible input cardinal states, storing them for 300 ns in the atom, and then reading them out by sending a 'read' pulse (~0.05 photons on average) from port $|\uparrow_z\rangle_p$. The state of the output photon was then analysed on the same axis as the input. Specifically, these measurements were obtained by defining a different atomic detection criterion for the fixed-direction probe atom-to-photon experiments, one that is not conditioned on a reflected photon in the write pulse. This resulted in six photon–atom–photon data sets, which practically did not overlap (2%–8% overlap) with the atom-to-photon data presented in Fig. 2b (see Methods).

The results, shown in Fig. 3, yield an average measured fidelity of $\overline{\mathcal{F}}_{PAP} = 64.2(\pm3.4)\%$. Here we used the fact that the swap operation inherently includes a heralding mechanism—it outputs a photon that does not carry any information about the 'written' state (only about the previous state of the atom), but does provide the information that the sent photonic qubit had reached its destination. The presented measurements were accordingly heralded on the detection of a single photon in the writing pulse, thereby ruling out the ~45% probability of vacuum in the writing pulse. Without heralding, the measured average fidelity was 60.0(±1.3)%, in good agreement with our theoretical analysis (see Methods for further details).

Due to the Poissonian statistics of the writing pulse, the fidelities obtained from both measurements (heralded and unheralded) do not directly represent the fidelity for the double-swap operation for an ideal input state of a single photon (see Methods for comparison with the classical threshold). Yet by analysing these results together with the measured results of the atom-to-photon swap process (Fig. 2b), one can infer the fidelity of the photon-to-atom swap process assuming a perfect single-photon input (see Methods). The resulting average fidelities are $\overline{\mathcal{F}}_{PA} = 75.6(\pm4.6)\%$ and $\overline{\mathcal{F}}_{PA} = 73.3(\pm3.3)\%$ for same-axis and fixed-direction probe methods, respectively (Fig. 4a,b). These fidelities, as well as the atom-to-photon swap fidelities presented in Fig. 2, are above the classical threshold for a readout of a single qubit[32] and agree well with the theoretical prediction[15].

In our current experimental realization, both the fidelity and the efficiency (~70%) are limited mainly by the polarization of the transverse-magnetic mode (being not completely circular), position-dependent variations in *g* and the intrinsic linear loss of the WGM. While all of these parameters can be further optimized, the potential of this scheme is the fact that it can be applied to any material Λ-system coupled to a waveguide. As the SPRINT mechanism requires no preparations or control fields, it also does not require a priori knowledge of the timing or temporal shape of the incoming photon (as long as the pulses are significantly longer than Γ^{-1}), and the output pulse ideally mimics the temporal shape of the input one. This gate is therefore highly suitable for scalable,

'digital -circuit-like' quantum networks, in which the output photonic qubit from one node can immediately serve as the input to the next one. It can also serve as a building block for universal quantum gates such as $\sqrt{SWAP}$ (refs [16,17]) and controlled-phase[33], thereby providing a versatile platform for quantum communication and distributed quantum information processing.

Methods

Methods, including statements of data availability and any associated accession codes and references, are available at https://doi.org/10.1038/s41567-018-0241-6.

Received: 26 November 2017; Accepted: 5 July 2018;
Published online: 13 August 2018

References

1. Cirac, J. I., Zoller, P., Kimble, H. J. & Mabuchi, H. Quantum state transfer and entanglement distribution among distant nodes in a quantum network. *Phys. Rev. Lett.* **78**, 3221–3224 (1997).
2. Monroe, C. Quantum information processing with atoms and photons. *Nature* **416**, 238–246 (2002).
3. Kimble, H. J. The quantum internet. *Nature* **453**, 1023–1030 (2008).
4. Monroe, C. et al. Large-scale modular quantum-computer architecture with atomic memory and photonic interconnects. *Phys. Rev. A* **89**, 022317 (2014).
5. Duan, L.-M. & Kimble, H. J. Scalable photonic quantum computation through cavity-assisted interactions. *Phys. Rev. Lett.* **92**, 127902 (2004).
6. Boozer, A. D., Boca, A., Miller, R., Northup, T. E. & Kimble, H. J. Reversible state transfer between light and a single trapped atom. *Phys. Rev. Lett.* **98**, 193601 (2007).
7. Specht, H. P. et al. A single-atom quantum memory. *Nature* **473**, 190–193 (2011).
8. Reiserer, A., Kalb, N., Rempe, G. & Ritter, S. A quantum gate between a flying optical photon and a single trapped atom. *Nature* **508**, 237–240 (2014).
9. Tiecke, T. G. et al. Nanophotonic quantum phase switch with a single atom. *Nature* **508**, 241–244 (2014).
10. Kalb, N., Reiserer, A., Ritter, S. & Rempe, G. Heralded storage of a photonic quantum bit in a single atom. *Phys. Rev. Lett.* **114**, 220501 (2015).
11. Shomroni, I. et al. All-optical routing of single photons by a one-atom switch controlled by a single photon. *Science* **345**, 903–906 (2014).
12. Inomata, K. et al. Microwave down-conversion with an impedance-matched Λ system in driven circuit QED. *Phys. Rev. Lett.* **113**, 63604 (2014).
13. Rosenblum, S. et al. Extraction of a single photon from an optical pulse. *Nat. Photon.* **10**, 19–22 (2016).
14. Inomata, K. et al. Single microwave-photon detector using an artificial Λ-type three-level system. *Nat. Commun.* **7**, 12303 (2016).
15. Rosenblum, S., Borne, A. & Dayan, B. Analysis of deterministic swapping of photonic and atomic states through single-photon Raman interaction. *Phys. Rev. A* **95**, 33814 (2017).
16. Koshino, K., Ishizaka, S. & Nakamura, Y. Deterministic photon-photon $\sqrt{\text{SWAP}}$ gate using a Λ system. *Phys. Rev. A* **82**, 10301 (2010).
17. Koshino, K. et al. Tunable quantum gate between a superconducting atom and a propagating microwave photon. *Phys. Rev. Appl.* **7**, 064006 (2016).
18. Bouwmeester, D. et al. Experimental quantum teleportation. *Nature* **390**, 575–579 (1997).
19. Gao, W. et al. Quantum teleportation from a propagating photon to a solid-state spin qubit. *Nat. Commun.* **4**, 2744 (2013).
20. Takeda, S., Mizuta, T., Fuwa, M., van Loock, P. & Furusawa, A. Deterministic quantum teleportation of photonic quantum bits by a hybrid technique. *Nature* **500**, 315–318 (2013).
21. Haroche, S. & Raimond, J.-M. *Exploring the Quantum: Atoms, Cavities, and Photons* (Oxford Univ. Press, Oxford, 2006).
22. Thompson, R. J., Rempe, G. & Kimble, H. J. Observation of normal-mode splitting for an atom in an optical cavity. *Phys. Rev. Lett.* **68**, 1132–1135 (1992).
23. Nickerson, N. H., Li, Y. & Benjamin, S. C. Topological quantum computing with a very noisy network and local error rates approaching one percent. *Nat. Commun.* **4**, 1756 (2013).
24. Hacker, B., Welte, S., Rempe, G. & Ritter, S. A photon–photon quantum gate based on a single atom in an optical resonator. *Nature* **536**, 193–196 (2016).
25. Pinotsi, D. & Imamoglu, A. Single photon absorption by a single quantum emitter. *Phys. Rev. Lett.* **100**, 93603 (2008).
26. Lin, G. W., Zou, X. B., Lin, X. M. & Guo, G. C. Heralded quantum memory for single-photon polarization qubits. *EPL* **86**, 30006 (2009).
27. Bradford, M. & Shen, J.-T. Single-photon frequency conversion by exploiting quantum interference. *Phys. Rev. A* **85**, 43814 (2012).
28. Gea-Banacloche, J. & Wilson, W. Photon subtraction and addition by a three-level atom in an optical cavity. *Phys. Rev. A* **88**, 33832 (2013).
29. Junge, C., O'Shea, D., Volz, J. & Rauschenbeutel, A. Strong coupling between single atoms and nontransversal photons. *Phys. Rev. Lett.* **110**, 213604 (2013).
30. Lodahl, P. et al. Chiral quantum optics. *Nature* **541**, 473–480 (2017).
31. Aiello, A., Banzer, P., Neugebauer, M. & Leuchs, G. From transverse angular momentum to photonic wheels. *Nat. Photon.* **9**, 789–795 (2015).
32. Massar, S. & Popescu, S. Optimal extraction of information from finite quantum ensembles. *Phys. Rev. Lett.* **74**, 1259–1263 (1995).
33. Tokunaga, Y. & Koshino, K. A photon–photon controlled-phase gate using a Λ system. in *European Quantum Electronics Conf. Proc.* EB_P_7 (Optical Society of America, 2015).

Acknowledgements

Support from the Israeli Science Foundation, the Minerva Foundation and the Crown Photonics Center is acknowledged. This research was made possible in part by the historic generosity of the Harold Perlman family.

Author contributions

All authors contributed to the carrying out of the experiment, discussed the results and commented on the manuscript. O.B. and A.B. analysed the data. O.B., A.B., S.R. and B.D. contributed to the design and construction of the experimental set-up. O.B., A.B., S.R. and B.D. wrote the manuscript. O.B., A.B. and S.R. contributed equally to this work.

Competing interests

The authors declare no competing interests.

Additional information

Supplementary information is available for this paper at https://doi.org/10.1038/s41567-018-0241-6.

Reprints and permissions information is available at www.nature.com/reprints.

Correspondence and requests for materials should be addressed to B.D.

Publisher's note: Springer Nature remains neutral with regard to jurisdictional claims in published maps and institutional affiliations.

Methods

Experimental sequence. Acquisition of experimental data was performed by repeatedly (~1 Hz) releasing a cloud of ~90 million ^{87}Rb atoms laser-cooled to ~7 μK onto a silicon chip carrying WGM microsphere resonators, 7 mm below. Light was coupled to a chosen WGM of a single resonator by a tapered nanofibre (Fig. 1c). All of the optical input/output ports of the nanofibre included 97:3 beamsplitters that functioned as optical circulators by attenuating the input weak coherent pulses and highly transmitting the output photons (Fig. 1c). At each release of the atomic cloud, the SPCMs were triggered and photon detection events were recorded for 30 ms. During this time, all of the trapping beams were turned off and repeated sequences of pulses were sent in an interleaved pattern to the input ports of the nanofibre, both to detect the presence of an atom within the evanescent field of the WGM and to swap a photonic qubit into the atom or read it back (see below). The magneto-optical trap was then turned back on and the cloud regenerated and cooled again to ~7 μK using polarization-gradient cooling. Between each drop, the WGM resonance was scanned and locked to the $F=1 \rightarrow F'=1$ ^{87}Rb D_2 transition, on resonance with the probe. Cavity locking was performed by controlling the temperature of the chip using a thermo-electric cooling element combined with free-space illumination of the microsphere using a 532 nm laser with an output of a few milliwatts.

Atom detection and pulse sequence. For detection of the atoms and carrying out the swap gates, attenuated coherent pulses were sent to the nanofibre through two or three input ports, each corresponding to a different state on the photonic qubit sphere (Fig. 1c). Data were extracted and analysed from ten different experiments, each with a different pulse sequence combination (Supplementary Figs. 1 and 2). Generally, the sequence consisted of four detection pulses, each ~10 ns long and with a mean photon number of ~1.2, sent alternately from opposite directions on a chosen axis of the photonic Bloch sphere. The first was ~10% stronger than the others and was used to initialize the atom and not for detection. Subsequently, two weaker and longer pulses were sent: 'write' and 'read' (~0.8, ~0.05 photons respectively, both ~50 ns in width and 300 ns apart), and finally four more pulses, identical to the initial detection pulses. These were, in fact, also the beginning of the next sequence, serving as a re-initialization pulse and three detection pulses. The extremely low mean photon number in the swap-out pulse is meant to minimize the probability for the presence (and possible detection) of a second photon in the pulse, leading to failure of the readout process (the very rare probability for such an event was nonetheless taken into account in our analysis). All of the detection pulses are meant to toggle the state of the atom by SPRINT, each toggle leading to reflection of the incoming photon with high probability, thereby indicating the presence of an atom in the mode. Conditioning on the detection of a reflection event in at least three detection pulses, some before and some after the two swap pulses, indicates that an atom was present within the cavity mode at a probability that varied between 92.5% and 94.2%. The false detection probability was measured periodically by sending detection pulse sequences to the cavity after the atomic cloud had passed, before the next drop. This statistic was then used to correct our measured data. For the atom-to-photon swap experiments, the write pulse was used both for detection and for preparation by conditioning the measurement on a reflection of a photon from this pulse, which indicates with high probability a successful swap operation and therefore preparation of the atom in the chosen state. The seventh pulse (the first of the last four detection pulses) served as an erasure pulse, meant to re-initialize the state of the atom after the measurement, and was not used for detection, to prevent biasing of the atomic detection probability by the possible success or failure of the preceding swap operation. In the photon-to-atom swap experiments, no conditioning was performed on the initial atomic state. Overall, data were acquired from a total of ~86,000 detected atoms in over 610,000 experimental cycles. All pulses were generated and shaped using an intensity electro-optic modulator (Photline NIR-MX800-LN-10) controlled by an arbitrary-waveform generator (Tektronix AWG7052). The pulses were then split into three acousto-optic modulators, used for channelling pulses into the various input ports to the nanofibre (Fig. 1c) with > 30 dB extinction ratio.

Data analysis. Data were collected using a total of ten SPCMs (six Excelitas SPCM-AQRH-14-FC and four additional modules in a Perkin-Elmer SPCM-AQ4C-FC array), and recorded using a photon correlator (Becker & Hickl DPC-230). To nullify any SPCM after-pulsing effects in our analysis, we disregard any detections that were separated by less than 200 ns on a given module. This, in turn, lowers the detection efficiency of additional photons within that time frame. Due to the close proximity of our detection pulses, the efficiency of our atom-detection process greatly depends on the number of active detectors at any given moment. To improve performance, we have therefore split both output channels of our apparatus and directed them into five SPCMs on each side (Fig. 1c). Additionally, we designed our pulse sequences so that the two swap pulses begin > 200 ns after the end of the detection pulses and are spaced by more than 200 ns (tail-to-tail) from each other as well (> 300 ns peak-to-peak).

Linear loss and single-photon detection efficiencies. The transmission of the bare tapered fibre was 90%, the optical-path efficiency starting from the output of the fibre to the detectors was 61.5% and the detection efficiency of the SPCMs ranged between 55% and 60%. The linear cavity loss of ~30% and atomic spontaneous emission to free space were the only optical losses that were considered inherent to this realization of the swap gate. During some of our 'pole' measurements, there was an additional asymmetric loss of 20%–34% caused by a defect that formed on our nanofibre to one side of the cavity. By continuously monitoring the residual reflection from the empty cavity in both directions and comparing them to each other and to the overall transmission, we were able to compensate for this loss and correct our results accordingly.

Inferring photon-to-atom swap fidelity. As described in the main text, using our measured experimental data, one can numerically infer the average photon-to-atom swap fidelity. We represent each single-swap process as a probability table, their combination yielding the double-swap fidelity. We define $P_{j,i}$ as the probability to j when expected to do i and denote $i,j=\{t,nt\}$ for atomic state 'toggle' or 'no toggle' and $i,j=\{R,T\}$ for photonic 'reflection' or 'transmission', respectively. As a first step, we deduced $P_{R,R}$ and $P_{T,T}$ from the experimental value $\overline{\mathcal{F}}_{AP}$ (Fig. 2b) and used them to generate all possible combinations for $P_{t,t}$ and $P_{nt,nt}$ and their return values $\overline{\mathcal{F}}'_{\mathrm{PAP}}$. Each pair was given a weight to quantify its result's proximity to the actual measured value $\overline{\mathcal{F}}_{PAP}$(Fig. 3). The next step used the previous $\{P_{t,t}, P_{nt,nt}\}$ table to calculate a new set of $P_{R,R}$ and $P_{T,T}$ values, together with weights, by comparing the return values $\overline{\mathcal{F}}'_{\mathrm{AP}}$ to the measured value $\overline{\mathcal{F}}_{AP}$. These two steps were repeated until they converged onto two sets of pairs $\{P_{t,t}, P_{nt,nt}\}$ and $\{P_{R,R}, P_{T,T}\}$ that were then used to calculate the average fidelities of the photon-to-atom ($\overline{\mathcal{F}}'_{\mathrm{PA}}$) and atom-to-photon ($\overline{\mathcal{F}}'_{\mathrm{AP}}$) swap processes, along with their respective errors. Performing this procedure with an atom initially populated at 50:50 and subsequently interacting with a series of detection and measurement pulses identical to our experimental sequence enables one to extract the average fidelity of our gate for a perfectly prepared atom and a true single-photon input. Throughout the calculation, realistic representation of pulses was carried out by assuming Poissonian photon-number distribution. Effectively, this meant applying the single-photon table according to the appropriate Poissonian probability for a single photon, applying it twice according to the probability for two-photons, or not applying anything according to the probability for vacuum.

False atomic preparation. Using the calculations described in the previous section, backed by measurements gathered from our previous experiments[13], we can quantify the false atomic preparation probability in our system with high accuracy. As stated in the main text, this is mostly attributed to crosstalk between the not completely circular transverse-magnetic modes[29]. This results in a ~4.5% probability to record a reflection in our detectors although the atom decays to the wrong ground state. Our swap-out results take these pre-measurement preparation errors into account.

Classical threshold of the swap gate. To ascertain the quantum nature of our swap gate, we must compare our measured average fidelity values to those obtainable in a classical system. Unlike a quantum process, a classical process initially involves projecting a general incoming quantum state onto a chosen axis. Assuming no prior knowledge of the incoming qubit axis, the highest achievable fidelity is therefore limited. Choosing the correct axis would project the state correctly, while the other two axes yield the correct state in only 50% of the cases. This sets the classical fidelity threshold for a readout of a single qubit[32] at 2/3. Our measured average atom-to-photon swap fidelities (74.7%–77.2%), as well as the photon-to-atom swap fidelities (73.3%–75.6%), inferred for a single-photon input), are above this limit.

Classical threshold of the swap-in–swap-out process. The double-swap operation consists of two independent processes that do not share any knowledge of their axis operation. Therefore, each of the operations should be limited to 2/3. The result of the double process in the classical case is therefore expected to be the sum of the probability for a correct swap in both directions (4/9) and the probability for two wrong swaps, which also leads to the correct result in 1/9 of the cases. For a true single-photon input, the classical limit is therefore 5/9 ~ 56% (if the write and read processes are allowed to share information about the chosen axis, the threshold remains 2/3). In the case of a coherent state with $n=0.8$, one must take into account the Poissonian nature of the input pulse[7]. For the heralded process, which rules out the possibility of vacuum input, this increases the classical threshold for the photon-to-atom swap to ~70% and the total threshold to ~57%. Our measured average photon–atom–photon fidelity in this case (64.2%) is above this limit as well.

Comparing heralded and unheralded results. The results for the double-swap and photon-to-atom swap experiments can be analysed for two possible modes of operation. One is heralding on the detection of a photon at the end of the writing stage, as discussed in the main text. This indicates both that the writing pulse had at least one photon, and that this photon was not lost after or (more importantly) before the interaction with the atom. Another mode of operation is the unheralded one, in which case the write pulse can sometimes be vacuum. As shown in Fig. 3, the average measured fidelity in the heralded case is $\overline{\mathcal{F}}_{PAP}=64.2(\pm3.4)\%$. The

unheralded average measured fidelity is 60.0(±1.3)%. Beyond the fact that in the unheralded case the writing pulse sometimes (~45%) contains no photons at all, in both cases there is also a probability that it had two photons or more. Inferring the fidelity of the same-axis photon-to-atom swap process for a perfect single-photon input, the resulting average fidelity is $\overline{\mathcal{F}}_{PA} = 75.3(\pm 4.6)\%$ in the heralded case (Fig. 4a) and 71.8(±3.8)% when unheralded. A difference of ~4% between these two numbers is indeed expected, resulting mostly from the 30% probability for linear loss of the write photon within the cavity, which in half of the cases occurs before it reaches the atom, and brings the expected photon-to-atom swap fidelity to that of vacuum, namely 50%. For the same process but with a fixed-direction probe, the average fidelity obtained is $\overline{\mathcal{F}}_{PA} = 73.3(\pm 3.3)\%$ when heralded (Fig. 4b) and 66.6(±2.1)% when unheralded.

Data availability. The data that support the plots within this paper and other findings of this study are available from the corresponding author upon reasonable request.